



Lagrangian Observation of ^{234}Th and Its Application in Constraining the Sinking of Particulate Organic Carbon on the Slope of the Northeastern South China Sea

Weifeng Yang^{1,2*}, Xiufeng Zhao^{1,2}, Min Chen², Yusheng Qiu² and Minfang Zheng²

¹ State Key Laboratory of Marine Environmental Science, Xiamen, China, ² College of Ocean and Earth Sciences, Xiamen University, Xiamen, China

OPEN ACCESS

Edited by:

Jixin Qiao,
Technical University of Denmark,
Denmark

Reviewed by:

Chin-Chang Hung,
National Sun Yat-sen University,
Taiwan
Hideki Fukuda,
The University of Tokyo, Japan

*Correspondence:

Weifeng Yang
wyang@xmu.edu.cn

Specialty section:

This article was submitted to
Marine Biogeochemistry,
a section of the journal
Frontiers in Marine Science

Received: 09 December 2021

Accepted: 27 January 2022

Published: 18 February 2022

Citation:

Yang W, Zhao X, Chen M, Qiu Y
and Zheng M (2022) Lagrangian
Observation of ^{234}Th and Its
Application in Constraining the Sinking
of Particulate Organic Carbon on
the Slope of the Northeastern South
China Sea. *Front. Mar. Sci.* 9:831937.
doi: 10.3389/fmars.2022.831937

The ^{234}Th – ^{238}U disequilibrium has been widely used to quantify the sinking flux of particulate organic carbon (POC) out of the upper ocean. However, the influence of the advection on the quantification is poorly understood due to the lack of *in situ* measured physical parameters. Here, a Lagrangian observation was deployed for 39 h to track the variability of ^{234}Th along with the current on the slope of the northeastern South China Sea (SCS). Contrasting to the general ocean interior, ^{234}Th showed deficits relative to ^{238}U in the mesopelagic waters, indicating an enhanced removal of ^{234}Th . Concurrently, elevated total particulate matter (TPM) and POC contents were observed in the mesopelagic waters, supporting the driving force of the cross-shelf dispersion of re-suspended shelf/slope sediments for the ^{234}Th removal. The widely used ^{234}Th -model (ignoring physical processes) produced a much lower sinking flux of POC than the sediment trap-derived POC flux during the same observation, indicating an unneglectable influence of advection and diffusion. By considering the main horizontal advection and vertical diffusion, the ^{234}Th – ^{238}U method gave rise to comparable results to sediment trap. ^{234}Th -derived POC fluxes showed an increased pattern from 300 to 1,000 m, consistent with the more abundant POC where. These results indicated that advection represents an unneglectable process during the quantification of the sinking flux of ^{234}Th over the slope of the SCS.

Keywords: thorium-234, mesopelagic water, export flux, resuspension, South China Sea

INTRODUCTION

Particulate organic carbon (POC) settling largely dominates the ability of the oceans to sequester carbon dioxide. Various types of sediment traps have been used to directly determine the flux of POC (Li et al., 2018; Shih et al., 2020). Due to the requirements of long collection time (≥ 24 h), professional technique, and manpower for deployment and recovery of sediment traps, the radioactive method of ^{234}Th – ^{238}U has later been developed and widely used in past decades (Buesseler et al., 2020). ^{234}Th ($T_{1/2} = 24.1$ days), naturally generated from its parent of ^{238}U , is a typical particle-reactive radionuclide in seawater (Black et al., 2018). Owing to its sinking with particles, ^{234}Th is usually deficient to ^{238}U in the upper

ocean (Roca-Martí et al., 2017; Umhau et al., 2019). This deficit has thus been used to quantify the sinking flux of particulate components (especially POC) out of the euphotic zone (Buesseler et al., 2009; Maiti et al., 2016). In general, the mass balance model of ^{234}Th is applied to constrain its sinking flux. Owing to the difficulty in obtaining *in situ* physical parameters (e.g., current velocity, diffusion coefficient, etc.) and collecting up-downstream gradient of ^{234}Th , the widely adopted model usually neglects advection and diffusion processes (Coppola et al., 2002; Yang et al., 2016, 2021a). A few studies indicate that physical processes can largely affect the ^{234}Th and POC fluxes in some oceanic settings, e.g., upwelling in the Equatorial Pacific (Bacon et al., 1996) and anticyclonic eddies (Zhou et al., 2013). In marginal seas and shallow waters with dynamic currents and tides, advection, and diffusion are expected to have a larger influence on the sinking flux of ^{234}Th (Zhao et al., 2019). In addition, steady-state is often assumed to quantify the flux of ^{234}Th due to the lack of time-series observation. However, non-steady-state, to a varying degree, influences the flux calculation (Martin et al., 2011; Resplandy et al., 2012). Besides, the ratio of POC to particulate ^{234}Th used to convert ^{234}Th flux to POC flux is another factor influencing the ^{234}Th - ^{238}U method. It is generally expected that POC/ ^{234}Th on large particles ($>50\ \mu\text{m}$) represent sinking particles. However, results from sediment traps reveal that ^{234}Th is mainly carried by small sinking particles (~ 70 – 80% of the total) in the northern South China Sea (SCS), representing the majority sinking of ^{234}Th (Hung et al., 2012). Less than $50\ \mu\text{m}$ particles account for most of the bulk POC in the northeastern SCS (Hung and Gong, 2010). The largest fractions of both ^{234}Th and POC in medium-sized (10 – $15\ \mu\text{m}$) particles are also observed in the northwestern Pacific Ocean (Hung et al., 2010). Hence, the influence of physical processes, temporal variability, and particle size on the ^{234}Th - ^{238}U method needs extensive investigations to improve the application of ^{234}Th - ^{238}U .

Usually, coastal and marginal seas show complicated hydrological conditions and significant spatiotemporal variability in the abundance of both ^{234}Th and POC (Feng et al., 2021a,b), which challenges the widely used advection-excluded ^{234}Th model (Zhao et al., 2019). Based on model-simulated physical parameters, i.e., advective velocity and diffusion coefficients, a few studies indicate that ignoring advection and diffusion would lead to a large deviation of ^{234}Th fluxes in some marginal seas, e.g., the basin of the SCS (Cai et al., 2008; Zhou et al., 2013). However, another study reports that including model-simulated physical parameters in ^{234}Th -model produces unreasonable results in the northern shelf/slope of the SCS due to the poorly constrained parameters (Cai et al., 2015). Thus, we hypothesize that dynamic hydrological fields result in the complex influence of physical processes on the quantification of ^{234}Th flux and ^{234}Th -derived POC flux in the shelf/slope areas. Thus, it is necessary to conduct *in situ* Lagrangian observation to obtain parameters and examine the influence of physical processes on the application of the ^{234}Th - ^{238}U method especially in oceanic settings with strong physical dynamics.

In this study, the northeastern SCS was selected to investigate the influence of horizontal advection on the estimation of ^{234}Th flux (Figure 1). Over the past decade, increasing studies report

the widely observed cross-shelf dispersion of particulate matter (Shih et al., 2019; Shen et al., 2020; Yang et al., 2021b; Ge et al., 2022) driven by the dynamic physical processes (Li et al., 2018; Jia et al., 2019). Thus, the northeastern SCS could be an ideal site for attesting to the influence of physical processes on the application of the ^{234}Th / ^{238}U method. Here, we conducted a Lagrangian observation of ^{234}Th on the northeastern slope of the SCS. The measured horizontal advection velocity and ^{234}Th in both upstream and downstream waters enable us to evaluate the influence of physical processes on the application of ^{234}Th in the SCS.

MATERIALS AND METHODS

Study Site

The study site is located in the northeastern SCS over the slope with water depths of hundreds of meters to more than a thousand meters (Figure 1). Recent researches have observed ubiquitous nepheloid layers (NLs) either in the mesopelagic water or in the bottom water of the northern SCS (Ma et al., 2017; Shih et al., 2019). A preliminary study indicates that internal solitary waves drive the resuspension of sediments on the slope (Jia et al., 2019). With the influence of currents, re-suspended particles disperse over a large scope as supported by the elevated particle fluxes in deeper sediment traps in the basin of the SCS (Schroeder et al., 2015; Hong et al., 2021). This dispersion of the shelf/slope sediments, mainly driven by advection, results in enhanced scavenging of particle-reactive nuclides (e.g., ^{210}Po) in the mesopelagic water of the SCS (Figure 3; Ma et al., 2017) and thus the sinking flux of POC (Yang et al., 2021b).

Sampling

The buoy, assembled a sediment trap array with three traps at 50, 100, and 200 m, was deployed from August 9 to 11, 2016 in the northeastern SCS (Figure 1). A Lagrangian observation was conducted, starting at station T1 and ending at station T2 with a duration of 39 h. Seawater was collected at both T1 and T2 from surface to 1,000 m (Table 1) using Niskin bottles attached to a conductivity, temperature, and depth (CTD)-rosette system aboard the *R/V Yanpin 2*. In brief, 8 L of seawater at each specific depth were collected and filtered through a pre-combusted (450°C for 4 h) and weighted quartz fiber (QMA) filter (WhatmanTM, Maidstone, United Kingdom). The total particulate matter (TPM) retained on the filter was de-salted using Milli-Q water for the measurements of particulate ^{234}Th ($^{234}\text{Th}_\text{p}$), POC, and TPM. Additionally, 4 L of the filtrate was collected for the analysis of dissolved ^{234}Th ($^{234}\text{Th}_\text{d}$). The euphotic zone of 0–150 m was determined by using a photosynthetically available radiation (PAR) scalar quantum irradiance sensor, defined as the depth of 0.1% of the surface light intensity.

^{234}Th and Total Particulate Matter Analyses

The particulate samples were dried at 60°C after collection and weighted to determine the difference between pure QMA filter

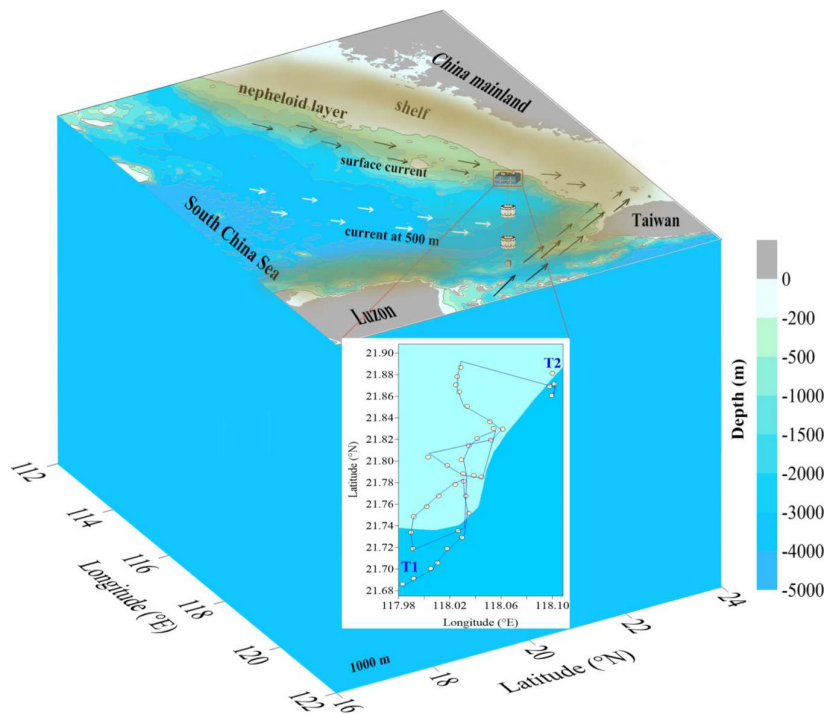


FIGURE 1 | Sampling stations in the northeastern South China Sea and the trajectory of the Lagrangian observation. The intervals between adjacent points denote the trajectory within an hour. The conceptual schematic of the nepheloid layer over the shelf/slope region highlights its ubiquity.

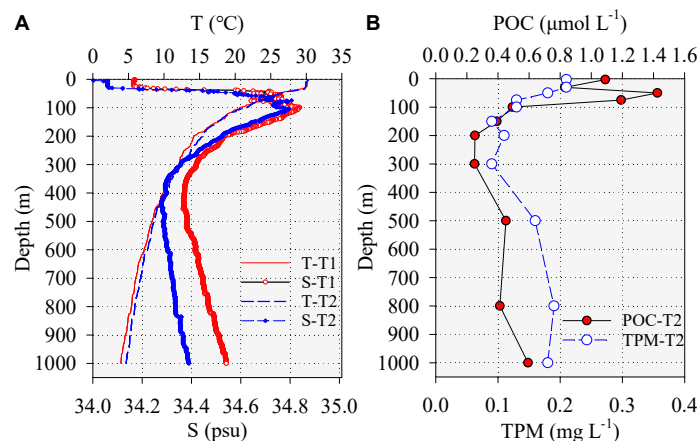


FIGURE 2 | Profiles of temperature, salinity at stations T1 and T2 (A), and particulate organic carbon (POC) and total particulate matter (TPM) at T2 (B).

and TPM-contained filter, i.e., the content of TPM. The activity of ²³⁴Th_P was counted using a gas-flow proportional low-level beta counter (RISØ GM-25-5A) as reported in our recent studies (Feng et al., 2021a,b) until the counting error was less than ±7%. A total of 150 days later, a second counting was conducted to assay the contribution of other beta emitters. ²³⁴Th_D in the filtrate was concentrated using the small volume MnO₂ co-precipitation method (Benitez-Nelson et al., 2001). In brief, the pH value of filtrate was adjusted to 9.0 using ammonium hydroxide, then KMnO₄ and MnCl₂ solution were added to form MnO₂

particles. After stirring and sanding for over 6 h to adsorb ²³⁴Th onto MnO₂ particles, MnO₂ precipitate was separated from the solution via filtration using a QMA filter. The average recovery was 94.7 ± 2.3%, showing a stable yield. Then, the sample was dried at 60°C, the activity of ²³⁴Th_D was counted using the same beta counter like ²³⁴Th_P but with < 5% counting error. The concentrations of both ²³⁴Th_D and ²³⁴Th_P were calculated based on the two measurements and corrected for recovery, blank counts, and sampling time. The activity concentrations of the total ²³⁸U were calculated using the newly updated ²³⁸U-salinity

relationship (Owens et al., 2011). The presented uncertainties of ^{234}Th were propagated from the counting errors. The total ^{234}Th ($^{234}\text{Th}_T$) and $^{234}\text{Th}/^{238}\text{U}$ ratio uncertainties were propagated from $^{234}\text{Th}_D$ and $^{234}\text{Th}_P$.

Particulate Organic Carbon Analysis

The Lagrangian observation was designed to constrain the *in situ* current velocity (horizontal advection) and the gradient of ^{234}Th activity between T1 and T2. On the northern SCS shelf with prominent cross-shelf transport of re-suspended sediments, this strategy could help us constrain the influence of advection on the flux estimation of ^{234}Th and ^{234}Th -derived POC flux at station T2. Hence, POC samples collected at station T2 were determined. After the measurements of $^{234}\text{Th}_P$, particulate-containing QMA filters were fumigated using concentrated HCl for no less than 48 h to remove inorganic carbon. Then, samples were dried at 60°C. POC content was measured using an elemental analyzer (Perkin Elmer CHN, Waltham, United States). The standard material used was IAEA-C8.

Particulate Organic Carbon Flux Calculation

The fluxes of TPM and POC was calculated from the ^{234}Th fluxes (Buesseler et al., 1992), i.e.,

$$F_{\text{TPM or POC}} = F_{\text{Th}} \times \frac{C_{\text{TPM or POC}}}{\text{Th}_P} \quad (1)$$

where F_{TPM} and F_{POC} represent the flux of TPM (in $\text{g m}^{-2} \text{day}^{-1}$) and POC (in $\text{mmol-C m}^{-2} \text{day}^{-1}$), respectively. C_{TPM} and C_{POC} are the concentrations of TPM and POC. Th_P denotes the activity concentration of $^{234}\text{Th}_P$.

RESULTS

Overall, the buoy floated northeast-ward along the surface current over the slope (Figure 1) with an average velocity of 19.5 cm s^{-1} , which is close to the mean of 15 cm s^{-1} obtained from the model simulation for the upper 200 m in the study area (Gan et al., 2006). At stations T1 and T2 sampled, it is clear that the difference in salinity was discernible though temperature showed little difference (Figure 2A), corresponding to water mixing during the transport of seawater from T1 to T2. The tracking of the movement of the buoy enables us to obtain the real viability of parameters along the trajectory of the buoy.

The concentrations of TPM varied from 0.09 to 0.21 mg L^{-1} with an average of $0.15 \pm 0.04 \text{ mg L}^{-1}$ (Figure 2B). POC concentrations showed a range of 0.25–1.42 $\mu\text{mol L}^{-1}$, averaging $0.67 \mu\text{mol L}^{-1}$. POC exhibited the highest values between 50 and 75 m (Figure 2B), corresponding to the widely observed depth of chlorophyll-a maximum in the SCS (Cai et al., 2015; Yang et al., 2021b). Notably, below the euphotic base (i.e., 150 m), both TPM and POC showed a downward increasing pattern (Figure 2B), increasing from 0.11 to 0.19 mg L^{-1} and 0.25 to 0.59 $\mu\text{mol L}^{-1}$, respectively. This phenomenon was also reported at a station near T1 during the same cruise (Yang et al., 2021b), pointing to the cross-shelf transport of re-suspended sediments.

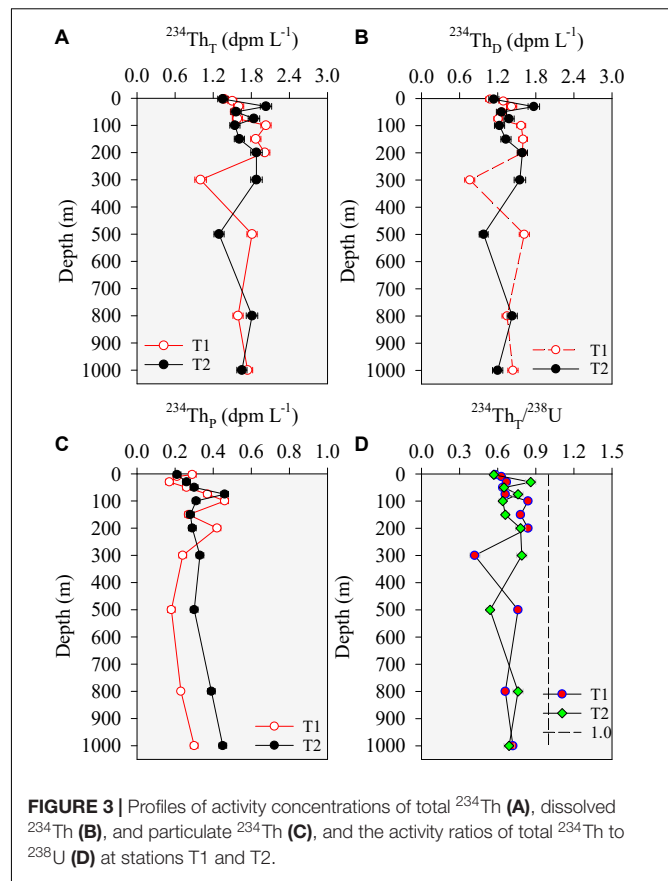


FIGURE 3 | Profiles of activity concentrations of total ^{234}Th (A), dissolved ^{234}Th (B), and particulate ^{234}Th (C), and the activity ratios of total ^{234}Th to ^{238}U (D) at stations T1 and T2.

The activity concentrations of $^{234}\text{Th}_T$ varied from 1.00 to 2.03 (avg.: 1.64 dpm L^{-1}) and 1.29–2.03 dpm L^{-1} (avg.: 1.68 dpm L^{-1}) at stations T1 and T2, respectively (Table 1 and Figure 3A). On average, $^{234}\text{Th}_D$ accounted for 67 and 63% of $^{234}\text{Th}_T$ at T1 and T2 (Figures 3B,C), coinciding with the major dissolved form of ^{234}Th in the open SCS (Zhou et al., 2013; Hong et al., 2021) and contrasting with the major particulate form in the coastal SCS (Feng et al., 2021a). The activity ratios of $^{234}\text{Th}_T$ to ^{238}U (i.e., $^{234}\text{Th}/^{238}\text{U}$) ranged from 0.42 to 0.84 at T1 and 0.54 to 0.86 at T2, averaging 0.67 and 0.70, respectively. Unlike the equilibrium between ^{234}Th and ^{238}U widely observed in mesopelagic waters, $^{234}\text{Th}/^{238}\text{U}$ showed deficits of ^{234}Th relative to ^{238}U at both T1 and T2 (Figure 3D), which was similar to the deficient ^{210}Po relative to ^{210}Pb observed near T1 during the same cruise (Yang et al., 2021b).

DISCUSSION

Influence of Cross-Shelf Process on ^{234}Th Profiles

$^{234}\text{Th}_T$ was lower than ^{238}U with the $^{234}\text{Th}/^{238}\text{U}$ ratios of 0.58–0.84 at T1 and 0.57–0.86 at T2 between surface and 150 m (Table 1), indicating an efficient removal of ^{234}Th from the euphotic zone (Figure 3). This observation is a typical scenario in the study area as was reported in all seasons (Cai et al., 2015).

TABLE 1 | Temperature, salinity, the content of total particulate matter (TPM), the concentration of particulate organic carbon (POC), activity concentrations of dissolved ^{234}Th ($^{234}\text{Th}_D$), particulate ^{234}Th ($^{234}\text{Th}_P$), total ^{234}Th ($^{234}\text{Th}_T$), and ^{238}U , and the activity ratios of $^{234}\text{Th}_T$ to ^{238}U during the Lagrangian observation from station T1 to station T2.

Stn.	Depth (m)	T (°C)	S (psu)	$^{234}\text{Th}_D$	$^{234}\text{Th}_P$			^{238}U	$^{234}\text{Th}_T/^{238}\text{U}$
					(dpm L ⁻¹)				
T1	3	30.25	34.17	1.08 ± 0.07	0.29 ± 0.02	1.37 ± 0.07	2.37	0.58 ± 0.03	
	10	30.11	34.17	1.29 ± 0.07	0.21 ± 0.01	1.50 ± 0.07	2.37	0.63 ± 0.03	
	30	29.76	34.21	1.42 ± 0.08	0.17 ± 0.02	1.60 ± 0.08	2.37	0.67 ± 0.03	
	50	25.95	34.67	1.27 ± 0.07	0.26 ± 0.02	1.54 ± 0.07	2.41	0.64 ± 0.03	
	75	23.98	34.66	1.21 ± 0.07	0.37 ± 0.02	1.58 ± 0.08	2.41	0.66 ± 0.03	
	100	20.64	34.84	1.57 ± 0.07	0.46 ± 0.02	2.03 ± 0.08	2.42	0.84 ± 0.03	
	150	17.59	34.72	1.60 ± 0.07	0.27 ± 0.02	1.87 ± 0.08	2.41	0.78 ± 0.03	
	200	14.21	34.53	1.59 ± 0.08	0.42 ± 0.02	2.01 ± 0.08	2.40	0.84 ± 0.03	
	300	12.11	34.42	0.76 ± 0.08	0.24 ± 0.02	1.00 ± 0.09	2.39	0.42 ± 0.04	
	500	8.31	34.38	1.62 ± 0.08	0.18 ± 0.02	1.81 ± 0.08	2.39	0.76 ± 0.03	
T2	800	5.40	34.47	1.35 ± 0.08	0.23 ± 0.01	1.59 ± 0.08	2.39	0.66 ± 0.03	
	1,000	3.94	34.54	1.44 ± 0.08	0.30 ± 0.02	1.74 ± 0.08	2.40	0.72 ± 0.03	
	3	30.21	34.16	1.14 ± 0.08	0.21 ± 0.02	1.35 ± 0.08	2.37	0.57 ± 0.03	
	30	29.88	34.21	1.77 ± 0.09	0.26 ± 0.02	2.03 ± 0.09	2.37	0.86 ± 0.04	
	50	26.14	34.58	1.26 ± 0.08	0.30 ± 0.02	1.56 ± 0.08	2.40	0.65 ± 0.03	
	75	23.81	34.78	1.38 ± 0.08	0.46 ± 0.02	1.84 ± 0.09	2.42	0.76 ± 0.04	
	100	21.50	34.81	1.23 ± 0.08	0.31 ± 0.02	1.54 ± 0.08	2.42	0.64 ± 0.03	
	150	17.40	34.75	1.33 ± 0.08	0.28 ± 0.02	1.61 ± 0.08	2.42	0.66 ± 0.03	
	200	15.37	34.58	1.59 ± 0.08	0.29 ± 0.02	1.88 ± 0.09	2.40	0.78 ± 0.04	
	300	12.48	34.41	1.55 ± 0.09	0.33 ± 0.02	1.88 ± 0.09	2.39	0.79 ± 0.04	
500	8.61	34.29	0.98 ± 0.07	0.30 ± 0.02	1.29 ± 0.08	2.38	0.54 ± 0.03		
800	5.88	34.36	1.43 ± 0.08	0.39 ± 0.02	1.81 ± 0.09	2.39	0.76 ± 0.04		
1,000	4.65	34.38	1.20 ± 0.08	0.45 ± 0.02	1.65 ± 0.08	2.39	0.69 ± 0.04		

Below the euphotic zone (200–1,000 m), the $^{234}\text{Th}_T$ deficits were also observed at both T1 and T2 with the $^{234}\text{Th}/^{238}\text{U}$ ratios of 0.42–0.84. Although ^{234}Th activity in the mesopelagic water of the SCS has not been reported, it is generally expected that ^{234}Th should reach equilibrium with ^{238}U due to the sparse TPM and long residence time of ^{234}Th . In fact, equilibrium states have been observed in most mesopelagic waters in the open oceans, e.g., the southeastern tropical Pacific (Black et al., 2018), the Atlantic Ocean (Owens and Buesseler, 2015), the Indian Ocean (Anand et al., 2018), and the Atlantic sector of the Southern Ocean (Roca-Martí et al., 2017). Considering the strong particle reactivity of ^{234}Th , the deficits of ^{234}Th were attributed to its enhanced removal along with TPM sinking in the mesopelagic waters at stations T1 and T2 (Figure 3). On the one hand, the elevated TPM and POC concentrations (Figure 2) provided direct evidence for the abundant particulate matter in mesopelagic water. Another particle-reactive radionuclide ^{210}Po also showed enhanced removal together with increased TPM in the mesopelagic water during the same cruise (Yang et al., 2021b). Shelf/slope sediment resuspension and successive dispersion are thought to be the provenance of the elevated TPM in the mesopelagic water of the northern SCS (Shih et al., 2019; Yang et al., 2021b), mechanistically driven by the internal solitary waves (Jia et al., 2019). On the other hand, abundant TPM usually leads to the deficits of ^{234}Th not only in the widely investigated euphotic zone but also in the less-studied ocean interior. For instance, evident ^{234}Th deficits have been observed in deep water near the active hydrothermal

vents (Yang et al., 2016, 2021a) and the hydrothermal plume (Owens and Buesseler, 2015). Thus, the deficits of ^{234}Th , together with the elevated TPM and POC contents in the mesopelagic water over the SCS slope, indicated that re-suspended sediments disperse over a large scope, supporting the influence of current advection on the spatial pattern of ^{234}Th in the study area.

The trajectory of the buoy revealed that seawater flows northeastward over the slope of the SCS (Figure 1). Station T1 was located upstream of the current, and T2 the downstream. Thus, the difference in ^{234}Th activities between T1 and T2 reflected the variability of ^{234}Th along the current, representing the real variation of ^{234}Th with time induced by its decay, generation from ^{238}U , and water exchange mainly horizontal advection as illustrated by the buoy movement. By taking advantage of the Lagrangian observation, these results enable us to evaluate the real advection flux of ^{234}Th and its influence on the sinking flux of ^{234}Th for the first time on the dynamic slope of the SCS.

Influence of Advection and Diffusion on the Sinking Flux of ^{234}Th

Ignoring the physical processes, the change of the amount of $^{234}\text{Th}_T$ with time can be expressed by:

$$\frac{dI_{ThT}}{dt} = \lambda_{Th} (I_U - I_{ThT}) - F_{Th} \quad (2)$$

where I_{ThT} and I_U are the inventories of the total ²³⁴Th and ²³⁸U from surface to the export depth (in dpm m⁻²), which are calculated through the trapezoidal integration method. λ_{Th} is the decay constant of ²³⁴Th (0.02876 day⁻¹). F_{Th} is the sinking flux of ²³⁴Th in dpm m⁻² day⁻¹. A sediment trap, deployed near station T2 on August 6, 2016, reports that the POC flux at 150 m was 8.4 ± 0.9 mmol-C m⁻² day⁻¹ (Li et al., 2018). The other array of sediment traps assembled to the buoy (from August 9 to 11, 2016) show the POC fluxes of 9.0 ± 0.6 mmol-C m⁻² day⁻¹ at 100 m and 9.3 ± 1.0 mmol-C m⁻² day⁻¹ at 200 m, respectively (Qiu, 2018). These consistent results indicated that particle sinking exhibited little variability during our sampling, lending support to the steady-state assumption. In addition, our sampling only covered 1.6 day, which could not enable the non-steady-state model to work well (Savoie et al., 2006). Thus, the steady-state is the best option in our study. At a steady-state, the sinking fluxes of ²³⁴Th estimated from Eq. (2) varied from 3,176 to 21,197 dpm m⁻² day⁻¹ [i.e., $\lambda_{Th}(I_U - I_{ThT})$ in Table 2]. The sinking flux of POC, estimated from Eq. (1), was 3.6 ± 0.3 mmol-C m⁻² day⁻¹ at 200 m, significantly lower than 9.3 ± 1.0 mmol-C m⁻² day⁻¹ determined by the sediment trap attached to the buoy (Qiu, 2018). Such an inconsistency indicated that physical processes, e.g., advection and diffusion, could be non-negligible during calculating the sinking flux of ²³⁴Th. Thus, the variability in total ²³⁴Th should be better expressed as:

$$\frac{dI_{ThT}}{dt} = \lambda_{Th}(I_U - I_{ThT}) + u \frac{\partial I_{ThT}}{\partial x} + k_z \frac{\partial A_{ThT}}{\partial z} - F_{Th} \quad (3)$$

where u and k_z denote the horizontal advection velocity of the total ²³⁴Th in cm s⁻¹ and vertical diffusive coefficient in cm² s⁻¹. $\partial I_{ThT}/\partial x$ and $\partial A_{ThT}/\partial z$ represent the gradient of inventory and activity of the total ²³⁴Th, respectively. To resolve Eq. (3), we need to assume (1) that the change rate of the inventory was uniform during the buoy transport; and (2) that the net changes of ²³⁴Th inventory were caused by the sinking of transported particles on the slope. For assumption (1), the consistent POC fluxes from two sediment traps (i.e., Li et al., 2018; Qiu, 2018) seemed to favor the little variability in the sinking flux of particles during our sampling. However, water mixing appeared to influence the second assumption. As shown in Figure 2, both temperature and salinity revealed the mixing of the traced water body with surrounding water masses during its transport from T1 to T2. The mixing processes of various waters, probably carrying

different ²³⁴Th contents, could affect the estimate of ²³⁴Th flux by changing the activity of ²³⁴Th. The influence was evaluated through the variations of both ²³⁴Th and ²³⁸U between T1 and T2 by taking ²³⁴Th decay into account. Results indicated that the mixing process accounted for <4% of the total ²³⁴Th fluxes (ignoring physical processes from Eq. 2) estimated in the upper 200 m. Below 200 m, mixing resulted in a large influence with an average of 18%. Although this influence seemed to be acceptable for the assumption (2), Eq. (3) is still not resolved due to the lack of advection velocity and spatial gradients of ²³⁴Th inventory.

The Lagrangian observation provided *in situ* velocity of current (i.e., 19.5 cm s⁻¹). However, this velocity is different from u in the second term on the right side of Eq. (3) in that particles have different transport speeds though basin-wide observations of sediment trap indicate that the transport of re-suspended sediment from the shelves is driven by lateral advection in the SCS (Schroeder et al., 2015). As an alternative strategy, we evaluated the influence of physical processes by comparing the flux of ²³⁴Th at 200 m (ignoring physical processes) with that calculated through trap-derived POC at 200 m (i.e., trap-POC flux divided by the C_{POC}/Th_p ratio in Eq. 1). The sinking flux of ²³⁴Th estimated from trap-POC flux was 10,775 ± 611 dpm m⁻² day⁻¹, which was much higher than 4,136 ± 148 dpm m⁻² day⁻¹ obtained by Eq. (2). In other words, physical processes resulted in 6,639 ± 629 dpm m⁻² day⁻¹ flux of ²³⁴Th. Although *in situ* observed velocity and the gradients of ²³⁴Th could not be directly applied to calculate the advection term in Eq. (3), they may, to a first-order approximation, be used to highlight the difference between the actual physical influence and our observations. The transport speed of particles is usually smaller than the current. If the observed velocity was used as an upper limit of the particle transport, and the derivative (i.e., the second term on the right side of Eq. 3) was substituted for the finite difference [i.e., $u(I_{ThT,T1} - I_{ThT,T2})/\Delta x$, commonly estimated from the linear interpolation, Resplandy et al., 2012], the upper limit of advection influence was estimated to be 4,733 ± 1,831 dpm m⁻² day⁻¹ at 200 m. The vertical gradients of the total ²³⁴Th (i.e., $\partial A_{ThT}/\partial z$) were estimated through the fitting curves obtained from its vertical distribution (Figure 3A), i.e., $A_{ThT} = 1.90e^{-0.0154z}$ ($r^2 = 0.82$) for 100–300 m. In the upper SCS, the diffusive coefficient ranges from 10⁻⁴ to 10⁻⁵ m² s⁻¹ even though it could reach 10⁻³ m² s⁻¹ in the mid-deep water (Wang et al., 2019). To evaluate the largest influence of the diffusion

TABLE 2 | Fluxes of ²³⁴Th_T and the fluxes of particulate organic carbon (POC) calculated from ²³⁴Th_T fluxes below the euphotic zone (150 m).

Depth (m)	$\lambda_{Th}(I_U - I_{ThT})$	$u(I_{ThT,T1} - I_{ThT,T2})/\Delta x$	$k_z(\partial A_{ThT}/\partial z)$	²³⁴ Th _T flux	POC/ ²³⁴ Th _p (μmol dpm ⁻¹)	POC flux (mmol-C m ⁻² day ⁻¹)	TPM flux (g m ⁻² day ⁻¹)
	(dpm m ⁻² day ⁻¹)						
150	3,176 ± 120	2,103 ± 1,478	251 ± 39	5,529 ± 1,484	1.41	7.8 ± 2.2	1.79 ± 0.11
200	4,136 ± 148	4,733 ± 1,831	116 ± 39	8,986 ± 1,837	0.86	7.8 ± 1.6	3.46 ± 0.20
300	5,628 ± 231	-2,636 ± 1,487	25 ± 38	3,016 ± 1,505	0.75	2.3 ± 1.1	0.84 ± 0.05
500	10,240 ± 407	-7,500 ± 2,703	120 ± 6	2,860 ± 2,734	1.48	4.2 ± 4.1	1.48 ± 0.09
800	17,422 ± 642	-1,526 ± 4,280	58 ± 6	15,954 ± 4,328	1.07	17.0 ± 4.7	7.70 ± 0.37
1,000	21,197 ± 730	-3,358 ± 4,834	36 ± 6	17,874 ± 4,889	1.32	23.7 ± 6.5	7.27 ± 0.30

TPM, total particulate matter.

term, we conservatively adopted $10^{-3} \text{ m}^2 \text{ s}^{-1}$. At 200 m, the estimated diffusion contribution to the sinking flux of ^{234}Th was $116 \pm 39 \text{ dpm m}^{-2} \text{ day}^{-1}$. Taken together, physical processes maximally accounted for $4,850 \pm 1,831 \text{ dpm m}^{-2} \text{ day}^{-1}$, lower than the actual physical effect of $6,639 \pm 629 \text{ dpm m}^{-2} \text{ day}^{-1}$. Since velocity was overestimated, the estimated lower flux indicated that there existed an addition of ^{234}Th from mixing or other processes during transport from T1 to T2, which led lower gradient and thus lower advection flux. It should be noted that although the product of the velocity of the buoy and the gradient of ^{234}Th accounted for the majority (73%) of the physical-contributed flux, it did not mean that Lagrangian observation provided actual physical parameters. Thus, Eq. (3) could not be completely resolved. Considering the fact that using these not-rigorous assumptions can present better results than those estimated by ignoring physical processes (Figure 4A), the observed data were used to constrain the fluxes of ^{234}Th and POC at other depths (Table 2). The results were compared with those obtained in the study area to further assay the rationality.

According to the model simulation (Gan et al., 2006), the current in the upper 200 m of the study area is somewhat different from that at 500 m. Simulated advection velocity of 10 cm s^{-1} below 200 m was adopted in calculating the advection flux of ^{234}Th . For diffusion, $^{234}\text{Th}_T$ followed $A_{ThT} = 1.90e^{-0.0154z}$ ($r^2 = 0.71$) between 500 and 1,000 m. The estimated flux for each process were presented in Table 2.

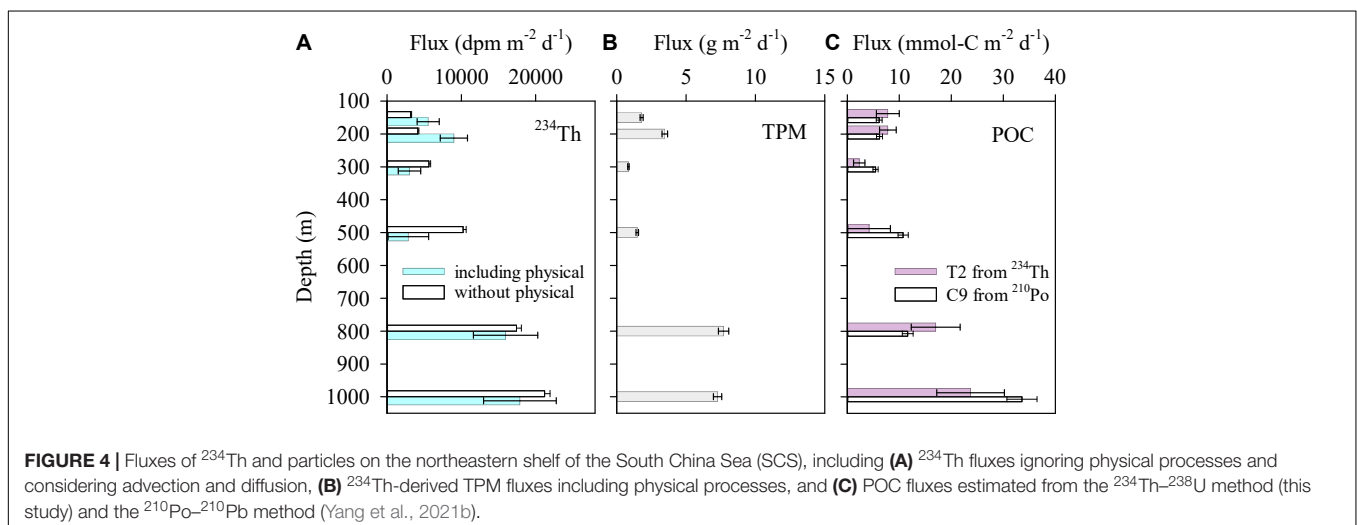
Export Fluxes of Total Particulate Matter and Particulate Organic Carbon Estimated From the Sinking Fluxes of ^{234}Th

The ^{234}Th -derived sinking fluxes of TPM varied from 0.88 to $7.70 \text{ g m}^{-2} \text{ day}^{-1}$, averaging $3.76 \text{ g m}^{-2} \text{ day}^{-1}$ at station T2 (Table 2). Over the western slope of the SCS, the ^{210}Po -derived sinking fluxes of TPM out of 1,000 m varied from 0.4 to $10.2 \text{ g m}^{-2} \text{ day}^{-1}$ with an average of $4.4 \text{ g m}^{-2} \text{ day}^{-1}$ (Ma et al., 2017). Our result of $7.27 \text{ g m}^{-2} \text{ day}^{-1}$ at 1,000 m fell within

this range. The minimum occurred at 300 m, corresponding to the low TPM contents (Figures 2, 4B). With the increasing of TPM content to the mesopelagic bottom (i.e., 1,000 m), TPM also showed elevated sinking fluxes, indicating the cross-shelf dispersion of re-suspended sediments.

At the base of the euphotic zone (150 m), the sinking flux of POC (collected from August 9 to 11, 2016) was $7.8 \text{ mmol-C m}^{-2} \text{ day}^{-1}$ (Table 2), very coincident with $8.4 \pm 0.9 \text{ mmol-C m}^{-2} \text{ day}^{-1}$ derived from a sediment trap near T2 (collected on August 6, 2016, Li et al., 2018), and falling in the range of sediment trap-derived scope of $2.8\text{--}9.0 \text{ mmol-C m}^{-2} \text{ day}^{-1}$ (Hung and Gong, 2010; Shih et al., 2019, 2020), satellite-derived $5.0\text{--}13.6 \text{ mmol-C m}^{-2} \text{ day}^{-1}$ (Chow et al., 2021), and ^{234}Th -derived scope of $4.6\text{--}11.8 \text{ mmol-C m}^{-2} \text{ day}^{-1}$ (Cai et al., 2015) in the northeastern SCS. In general, sediment trap directly collects particles, which largely represent the total effect of all processes including biogenic, physical, and chemical ones (Hung et al., 2016; Shih et al., 2019), though it is sometimes influenced by trapping efficiency (Coppola et al., 2002). The comparability between our results and published datasets also indicated that the considering physical processes produced better fluxes of particles than those ignoring physical processes. Owing to the requirements for technical expertise and high cost, the sediment traps are usually deployed with low spatial resolution. In contrast, the ^{234}Th method can provide POC flux data with high-resolution (Cai et al., 2008), but it suffers from poorly-constrained physical processes (Zhou et al., 2013). Biogeochemical models can decipher regional to global characteristics of POC flux, however, they often deviate from *in situ* measurements within small scope (Shih et al., 2021). Thus, accurate and high-resolution carbon export could be obtained in field studies by taking multiple methods' merits (Baker et al., 2020).

Conventionally, large particles ($>53 \mu\text{m}$) are assumed to be the representative of sinking particles for determining POC/ ^{234}Th ratios. However, some studies suggest that small particles ($<50 \mu\text{m}$) contribute the majority sinking of POC and ^{234}Th . For example, 1–10 and 10–50 μm fractions account



for 26–35 and 25–29% of the total POC based on the drifting sediment traps in the northern SCS (Hung and Gong, 2010). ^{234}Th carried by $<50\ \mu\text{m}$ particles contributes ~70–80% of the total ^{234}Th in the northwestern Pacific Ocean (Hung et al., 2010, 2012). These results thus lend support to the conclusion that particles collected in our study represent the majority of sinking particles in the northern SCS. In addition, the $\text{POC}/^{234}\text{Th}$ ratios varied from 0.75 to $1.48\ \mu\text{mol dpm}^{-1}$ (Table 2), which are comparable to $0.8\text{--}1.3\ \mu\text{mol dpm}^{-1}$ obtained on $1\text{--}50\ \mu\text{m}$ particles from sediment traps in the northern SCS (Hung and Gong, 2010), also supporting this conclusion. Notably, the POC flux out of the euphotic zone was much higher than those observed in the northern basin (Zhou et al., 2013) and the southern basin of the SCS (mostly $<5.0\ \text{mmol-C m}^{-2}\ \text{day}^{-1}$) (Cai et al., 2008; Yang et al., 2015), partly ascribed to the internal wave-induced input of nutrient-replete waters to the euphotic zone and successive phytoplankton flourish and POC settling (Li et al., 2018).

Compared with the flux at 150 m, POC showed comparable and significantly lower fluxes at 200 and 300 m, respectively (Table 2). In general, POC decreases with depth below the euphotic zone due to remineralization (Yang et al., 2009). Based on the ^{234}Th fluxes and $\text{POC}/^{234}\text{Th}$ ratios (Table 2), it is clear that $\text{POC}/^{234}\text{Th}$ ratios largely result in the flux descending with depth. Below 300 m, evident increases in POC flux occurred, from 4.2 to $23.7\ \text{mmol-C m}^{-2}\ \text{day}^{-1}$ (Figure 4C). Obviously, there are additional sources of POC besides its settling from local upper water. The vertical profile of TPM (Figure 2) illustrates additional contributions. Internal waves can lead to the resuspension of shelf/slope sediments in the northern SCS (Jia et al., 2019). Just before our sampling, strong internal waves were observed in the study area (Li et al., 2018). Probably, internal wave-induced resuspension of organic matter resulted in the elevated POC fluxes via cross-shelf dispersion. Similar scenarios were also observed at a station near T1 during the same cruise (Yang et al., 2021b) and in another study conducted in the same area (Shih et al., 2019). The scanning electron microscope images of the sinking particles below 150 m indicate a higher proportion of lithogenic material (Shih et al., 2019), lending support to its sediment origin.

A recent study reveals that a large amount of POC is required to support the consumption of deep microbes in the SCS interior (Shen et al., 2020). Our results provide direct evidence for the cross-transport of POC. Using the lowest value at 300 m as a reference, shelf/slope sediments contributed $1.7\text{--}21.3\ \text{mmol-C m}^{-2}\ \text{day}^{-1}$ to the mesopelagic waters of the SCS. At a station close to T1 during the same cruise, the sinking fluxes of POC were estimated to vary from 5.4 to $33.6\ \text{mmol-C m}^{-2}\ \text{day}^{-1}$ based on the $^{210}\text{Po}\text{--}^{210}\text{Pb}$ method (Yang et al., 2021b). Considering the uncertainties, the ^{210}Po -derived fluxes by neglecting the horizontal advection

and diffusion, were consistent with our ^{234}Th -derived results (Figure 4), indicating less influence of advection on the $^{210}\text{Po}\text{--}^{210}\text{Pb}$ method.

CONCLUSION

A Lagrangian observation of ^{234}Th was conducted over the slope of the northeastern SCS. Enhanced removal of ^{234}Th was observed in the mesopelagic waters compared with general mesopelagic oceans, pointing to the active particle dynamics below the euphotic zone of the SCS. Concurrently elevated TPM and POC concentrations with depth in the mesopelagic water revealed that re-suspended sediments from the shelf/slope dominated the removal of ^{234}Th . Combining the sediment trap results, the influence of physical processes on the sinking flux estimates of ^{234}Th was evaluated, revealing unneglectable effects of horizontal advection and vertical diffusion. Although considering the physical processes seemed to produce better sinking fluxes of ^{234}Th and POC, well-constraining the advection effect is still challenging due to the difficulty in obtaining the actual transport velocity of particles and spatial gradients.

DATA AVAILABILITY STATEMENT

The original contributions presented in the study are included in the article/supplementary material, further inquiries can be directed to the corresponding author.

AUTHOR CONTRIBUTIONS

XZ, YQ, and MZ collected and analyzed the samples. WY conceived and wrote the manuscript. MC edited the manuscript. All authors approved the submitted version.

FUNDING

This study was financially supported by the National Natural Science Foundation of China (Grant Nos. 42076030 and 41476061 to WY). Data and samples were collected onboard of *R/V “Yanping 2”* implementing the open research cruise NORC2016-04 supported by NSFC Shiptime Sharing Project (Grant No. 41549904).

ACKNOWLEDGMENTS

We thank the reviewers and editors for their constructive suggestions. We also thank YQ for his technical assistance during field observation and crew members of the *R/V Yanping 2* for their help during sample collection.

REFERENCES

- Anand, S. S., Rengarajan, R., and Sarma, V. V. S. S. (2018). ^{234}Th -based carbon export flux along the Indian GEOTRACES LI02 section in the Arabian Sea and the Indian Ocean. *Glob. Biogeochem. Cy.* 32, 417–436. doi: 10.1002/2017GB005847
- Bacon, M. P., Cochran, J. K., Hirschberg, D., Hammar, T. R., and Fleer, A. P. (1996). Export flux of carbon at the equator during the EqPac time-series cruises estimated from ^{234}Th measurements. *Deep Sea Res. II* 43, 1133–1153. doi: 10.1016/0967-0645(96)00016-1
- Baker, C. A., Estapa, M. L., Iversen, M., Lampitt, R., and Buesseler, K. O. (2020). Are all sediment traps created equal? An intercomparison study of carbon export methodologies at the PAP-SO site. *Progr. Oceanogr.* 184:102317. doi: 10.1016/j.pocan.2020.102317
- Benitez-Nelson, C. R., Buesseler, K. O., Rutgers van der Loeff, M. M., Andrews, J., Ball, L., Crossin, G., et al. (2001). Testing a new small-volume technique for determining ^{234}Th in seawater. *J. Radioanal. Nucl. Chem.* 248, 795–799. doi: 10.1023/A:1010621618652
- Black, E. E., Buesseler, K. O., Pike, S. M., and Lam, P. J. (2018). ^{234}Th as a tracer of particulate export and remineralization in the southeastern tropical Pacific. *Mar. Chem.* 201, 35–50. doi: 10.1016/j.marchem.2017.06.009
- Buesseler, K. O., Bacon, M. P., Cochran, J. K., and Livingston, H. D. (1992). Carbon and nitrogen export during the JGOFS North Atlantic bloom experiment estimated from ^{234}Th : ^{238}U disequilibria. *Deep-Sea Res. I* 39, 1115–1137. doi: 10.1016/0198-0149(92)90060-7
- Buesseler, K. O., Benitez-Nelson, C. R., Roca-Martí, M., Wyatt, A. M., Resplandy, L., Clevenger, S. J., et al. (2020). High-resolution spatial and temporal measurements of particulate organic carbon flux using ^{234}Th in the northeast Pacific Ocean during the export processes in the ocean from RemoTe Sensing field campaign. *Elem. Sci. Anth.* 8:1. doi: 10.1525/elementa.030
- Buesseler, K. O., Pike, S., Maiti, K., Lamborg, C. H., Siegel, D. A., and Trull, T. W. (2009). ^{234}Th as a tracer of spatial, temporal and vertical variability in particle flux in the North Pacific. *Deep Sea Res. I* 56, 1143–1167. doi: 10.1016/j.dsr.2009.04.001
- Cai, P., Chen, W., Dai, M., Wan, Z., Wang, D., Li, Q., et al. (2008). A high-resolution study of particle export in the southern South China Sea based on ^{234}Th : ^{238}U disequilibrium. *J. Geophys. Res.* 113:C04019. doi: 10.1029/2007JC004268
- Cai, P., Zhao, D., Wang, L., Huang, B., and Dai, M. (2015). Role of particle stock and phytoplankton community structure in regulating particulate organic carbon export in a large marginal sea. *J. Geophys. Res. Oceans* 120, 2063–2095. doi: 10.1002/2014JC010432
- Chow, C. H., Shih, Y.-Y., Chien, Y.-T., Chen, J. Y., Fan, N., Wu, W.-C., et al. (2021). The wind effect on biogeochemistry in eddy cores in the northern South China Sea. *Front. Mar. Sci.* 8:717576. doi: 10.3389/fmars.2021.717576
- Coppola, L., Roy-Barman, M., Wassmann, P., Mulsow, S., and Jeandel, C. (2002). Calibration of sediment traps and particulate organic carbon export using ^{234}Th in the Barents Sea. *Mar. Chem.* 80, 11–26. doi: 10.1016/S0304-4203(02)00071-3
- Feng, N., Yang, W., Zhao, X., Chen, M., Qiu, Y., and Zheng, M. (2021a). Seasonal export of ^{234}Th and POC in Daya Bay, northern South China Sea. *Cont. Shelf Res.* 216:104359. doi: 10.1016/j.csr.2021.104359
- Feng, N., Yang, W., Zhao, X., Chen, M., Qiu, Y., and Zheng, M. (2021b). Semi-enclosed bays serve as hotspots for black carbon burial: a case study in Jiaozhou Bay, western Yellow Sea. *Sci. Total Environ.* 797:149100. doi: 10.1016/j.scitotenv.2021.149100
- Gan, J., Li, H., Curchitser, E. N., and Haidvogel, D. B. (2006). Modeling South China Sea circulation: response to seasonal forcing regimes. *J. Geophys. Res.* 111:C06034. doi: 10.1029/2005JC003298
- Ge, Z., Li, Q. P., Yang, W., Liu, X., and Wu, Z. (2022). Transparent exopolymer particle dynamics along a shelf-to-sea gradient and impacts on the regional carbon cycle. *Sci. Total Environ.* 808:152117. doi: 10.1016/j.scitotenv.2021.152117
- Hong, Q., Peng, S., Zhao, D., and Cai, P. (2021). Cross-shelf export of particulate organic carbon in the northern South China Sea: insights from a ^{234}Th mass balance. *Progr. Oceanogr.* 193:102532. doi: 10.1016/j.pocan.2021.102532
- Hung, C.-C., Chen, Y.-F., Hsu, S.-C., Wang, K., Chen, J., and Burdige, D. J. (2016). Using rare earth elements to constrain particulate organic carbon flux in the East China Sea. *Sci. Rep.* 6:33880. doi: 10.1038/srep33880
- Hung, C.-C., and Gong, G.-C. (2010). POC/ ^{234}Th ratios in particles collected in sediment traps in the northern South China Sea. *Estuar. Coast. Shelf Sci.* 88, 303–310. doi: 10.1016/j.ecss.2010.04.008
- Hung, C.-C., Gong, G.-C., and Santschi, H. (2012). ^{234}Th in different size classes of sediment trap collected particles from the Northwestern Pacific Ocean. *Geochim. Cosmochim. Acta* 91, 60–74. doi: 10.1016/j.gca.2012.05.017
- Hung, C.-C., Xu, C., Santschi, P. H., Zhang, S.-J., Schwehr, K. A., Quigg, A., et al. (2010). Comparative evaluation of sediment trap and ^{234}Th -derived POC fluxes from the upper oligotrophic waters of the Gulf of Mexico and the subtropical northwestern Pacific Ocean. *Mar. Chem.* 121, 132–144. doi: 10.1016/j.marchem.2010.03.011
- Jia, Y., Tian, Z., Shi, X., Liu, J. P., Chen, J., and Liu, X. (2019). Deep-sea sediment resuspension by internal solitary waves in the Northern South China Sea. *Sci. Rep.* 9:12137. doi: 10.1038/s41598-019-47886-y
- Li, D., Chou, W.-C., Shih, Y.-Y., Chen, G.-Y., Chang, Y., Chow, C. H., et al. (2018). Elevated particulate organic carbon export flux induced by internal waves in the oligotrophic northern South China Sea. *Sci. Rep.* 8:2042. doi: 10.1038/s41598-018-20184-9
- Ma, H., Yang, W., Zhang, L., Zhang, R., Chen, M., Qiu, Y., et al. (2017). Utilizing ^{210}Po deficit to constrain particle dynamics in mesopelagic water, western South China Sea. *Geochem. Geophys. Geosyst.* 18, 1594–1607. doi: 10.1002/2017GC006899
- Maiti, K., Bosu, S., Dsa, E. J., Adhikari, P. L., Sutor, M., and Longnecker, K. (2016). Export fluxes in northern Gulf of Mexico—comparative evaluation of direct, indirect and satellite-based estimates. *Mar. Chem.* 184, 60–77. doi: 10.1016/j.marchem.2016.06.001
- Martin, P., Lampitt, R. S., Perry, J. J., Sanders, R., Lee, C., and D'Asaro, E. (2011). Export and mesopelagic particle flux during a North Atlantic spring diatom bloom. *Deep Sea Res. I* 58, 338–349. doi: 10.1016/j.dsr.2011.01.006
- Owens, S. A., and Buesseler, K. O. (2015). ^{234}Th as a tracer of particle dynamics and upper ocean export in the Atlantic Ocean. *Deep Sea Res. II* 116, 42–59. doi: 10.1016/j.dsr2.2014.11.010
- Owens, S. A., Buesseler, K. O., and Sims, K. W. W. (2011). Re-evaluating the ^{238}U salinity relationship in seawater: implications for the ^{238}U - ^{234}Th disequilibrium method. *Mar. Chem.* 127, 31–39. doi: 10.1016/j.marchem.2011.07.005
- Qiu, Y. (2018). *Regulatory Mechanism of Plankton Community Structure on Particulate Organic Carbon Export in Different Ecosystems of Subtropical Marginal Seas*. Ph.D. Dissertation. Xiamen: Xiamen University, 42–65.
- Resplandy, L., Martin, A. P., Le Moigne, F., Martin, P., Aquilina, A., Mémery, L., et al. (2012). How does dynamical variability impact ^{234}Th -derived estimates of organic export? *Deep Sea Res. I* 68, 24–45. doi: 10.1016/j.dsr2012.05.015
- Roca-Martí, M., Puigcorbó, V., Iversen, M. H., Rutgers van der Loeff, M., Klaas, C., Cheah, W., et al. (2017). High particulate organic carbon export during the decline of a vast diatom bloom in the Atlantic sector of the Southern Ocean. *Deep Sea Res. II* 138, 102–115. doi: 10.1016/j.dsr2.2015.12.007
- Savoie, N., Benitez-Nelson, C., Burd, A. B., Cochran, J. K., Charette, M., Buesseler, K. O., et al. (2006). ^{234}Th sorption and export models in the water column: a review. *Mar. Chem.* 100, 234–249. doi: 10.1016/j.marchem.2005.10.014
- Schroeder, A., Wiesner, M. G., and Liu, Z. (2015). Fluxes of clay minerals in the South China Sea. *Earth Planet. Sci. Lett.* 430, 30–42. doi: 10.1016/j.epsl.2015.08.001
- Shen, J., Jiao, N., Dai, M., Wang, H., Qiu, G., Chen, J., et al. (2020). Laterally transported particles from margins serve as a major carbon and energy source for dark ocean ecosystems. *Geophys. Res. Lett.* 47:e2020GL088971. doi: 10.1029/2020GL088971
- Shih, Y.-Y., Hung, C.-C., Tuo, S.-H., Shao, H.-J., Chow, C. H., Muller, F. L. L., et al. (2020). The impact of eddies on nutrient supply, diatom biomass and carbon export in the northern South China Sea. *Front. Earth Sci.* 8:537332. doi: 10.3389/feart.2020.537332
- Shih, Y.-Y., Lin, H.-H., Li, D., Hsieh, H.-H., Hung, C.-C., and Chen, C.-T. A. (2019). Elevated carbon flux in deep waters of the South China Sea. *Sci. Rep.* 9:1496. doi: 10.1038/s41598-018-37726-w
- Shih, Y.-Y., Shiah, F.-K., Lai, C.-C., Chou, W.-C., Tai, J.-H., Wu, Y.-S., et al. (2021). Comparison of primary production using in situ and satellite-derived values at the SEATS station in the South China Sea. *Front. Mar. Sci.* 8:747763. doi: 10.3389/fmars.2021.747763

- Umhau, B. P., Benitez-Nelson, C. R., Close, H. G., Hannides, C. S., Motta, L., Popp, B. N., et al. (2019). Seasonal and spatial changes in carbon and nitrogen fluxes estimated using ^{234}Th / ^{238}U disequilibria in the North Pacific tropical and subtropical gyre. *Mar. Chem.* 217:103705. doi: 10.1016/j.marchem.2019.103705
- Wang, D., Wang, Q., Cai, S., Shang, X., Peng, S., Shu, Q., et al. (2019). Advances in research of the mid-deep South China Sea circulation. *Sci. China Earth Sci.* 62, 1992–2004. doi: 10.1007/s11430-019-9546-3
- Yang, W., Chen, M., Zheng, M., He, Z., Zhang, X., Qiu, Y., et al. (2015). Influence of a decaying cyclonic eddy on biogenic silica and particulate organic carbon in the tropical South China Sea based on ^{234}Th / ^{238}U disequilibrium. *PLoS One* 10:e0136948. doi: 10.1371/journal.pone.0136948
- Yang, W., Huang, Y., Chen, M., Qiu, Y., Peng, A., and Zhang, L. (2009). Export and remineralization of POM in the Southern Ocean and the South China Sea estimated from $^{210}\text{Po}/^{210}\text{Pb}$ disequilibria. *Chin. Sci. Bull.* 54, 2118–2123. doi: 10.1007/s11434-009-0043-4
- Yang, W., Zhang, X., Chen, M., Fang, Z., and Qiu, Y. (2021a). Utilizing $^{234}\text{Th}/^{238}\text{U}$ disequilibrium to constrain particle dynamics in hydrothermal plumes in the Southwest Indian Ocean. *Acta Oceanol. Sin.* 40, 16–25. doi: 10.1007/s13131-021-1786-2
- Yang, W., Zhao, X., Guo, L., Huang, B., Chen, M., Fang, Z., et al. (2021b). Utilization of soot and ^{210}Po - ^{210}Pb disequilibria to constrain POC fluxes in the northeastern South China Sea. *Front. Mar. Sci.* 8:694428. doi: 10.3389/fmars.2021.694428
- Yang, W., Zhang, X., Chen, M., and Qiu, Y. (2016). Unusually low ^{234}Th in a hydrothermal effluent plume over the Southwest Indian Ridge. *Geochim. Geophys. Geosyst.* 17, 3815–3824. doi: 10.1002/2016GC006580
- Zhao, X., Yang, W., Ma, H., Li, J., Chen, M., Fang, Z., et al. (2019). Seasonal variations in the abundance and sinking flux of biogenic silica in Daya Bay, northern South China Sea. *Oceanologia* 61, 239–251. doi: 10.1016/j.oceano.2018.2018
- Zhou, K., Dai, M., Kao, S.-J., Wang, L., Xiu, P., Chai, F., et al. (2013). Apparent enhancement of ^{234}Th -based particle export associated with anticyclonic eddies. *Earth Planet. Sci. Lett.* 381, 198–209. doi: 10.1016/j.epsl.2013.07.039

Conflict of Interest: The authors declare that the research was conducted in the absence of any commercial or financial relationships that could be construed as a potential conflict of interest.

Publisher's Note: All claims expressed in this article are solely those of the authors and do not necessarily represent those of their affiliated organizations, or those of the publisher, the editors and the reviewers. Any product that may be evaluated in this article, or claim that may be made by its manufacturer, is not guaranteed or endorsed by the publisher.

Copyright © 2022 Yang, Zhao, Chen, Qiu and Zheng. This is an open-access article distributed under the terms of the Creative Commons Attribution License (CC BY). The use, distribution or reproduction in other forums is permitted, provided the original author(s) and the copyright owner(s) are credited and that the original publication in this journal is cited, in accordance with accepted academic practice. No use, distribution or reproduction is permitted which does not comply with these terms.